now published as:
I. Vecchi, A. Arcioni, C. Bacchiocchi, G. Tiberio, P. Zanirato, C. Zannoni,
Expected and unexpected behavior of the orientational order and dynamics induced by azobenzene solute
J. Phys. Chem. B, 111, 3355-3362 (2007)

Expected and unexpected behavior of the orientational order and dynamics induced by azobenzene solutes in a nematic

Ilaria Vecchi[a], Alberto Arcioni[a], Corrado Bacchiocchi[a], Giustiniano Tiberio[a], Paolo Zanirato[b] and Claudio Zannoni*[,a]

[a] *Dipartimento di Chimica Fisica e Inorganica and INSTM, Università, Viale Risorgimento 4, I-40136 Bologna, Italy*

[b] *Dipartimento di Chimica Organica "A. Mangini", Università, Viale Risorgimento 4, I-40136 Bologna, Italy*

* Corresponding Author: Fax: + 39 051 644 7012.
E-mail: Claudio.Zannoni@unibo.it.
URL: http://www.fci.unibo.it/~bebo/z/.

Abstract

We have explored the changes in the phase stability, orientational order and dynamics of the nematic 4-cyano-4′-n-pentylbiphenyl (5CB) doped with either the *trans* or the *cis* form of different *p*-azobenzene derivatives using the ESR spin probe technique. In particular, we have studied the effects induced by each of the seven non-mesogenic 4-R-phenylazobenzenes (R = H, F, Br, CH_3, CF_3, O*n*-Bu, O*t*-Bu) at 1% and 7% mole fraction on the order parameter $\langle P_2 \rangle$ and on the shift of the nematic–isotropic transition temperature (T_{NI}), as reported by a nitroxide spin probe, and we have tried to relate them to the solute shape and charge distribution. In all the cases the presence of the azo-derivative causes a depression of T_{NI}, more pronounced for the *cis* isomers. The dependence of $\langle P_2 \rangle$ on the reduced temperature $T^* = T/T_{NI}$ remains the same as that of pure 5CB in all *trans*-doped samples at 1% and 7% and decreases only slightly in the *cis* at 1%. However, we observe different and in some cases large variations (up to 25%) in $\langle P_2 \rangle$ for the *cis* at 7%, showing solute effects that go beyond the shift in T_{NI}. Surprisingly enough, even at the highest concentration, the probe dynamics appears to be essentially independent of the nature, the configuration and the concentration of the different solutes and very similar to that observed in the pure 5CB.

Keywords: *liquid crystals, ESR spin probe, biphasic systems, complex fluids, optical materials, photoisomerization*

Introduction

The orientational order, the dynamics and in general the physical properties of nematic liquid crystals (LC's) are influenced by dissolved solutes.[1–3] The most obvious manifestation is the disruption of alignment induced by spherical solutes, leading to a lowering of the nematic–isotropic phase transition temperature T_{NI}.[4] The effects on the medium are, however, related to the molecular features of the solutes (shape, dipole moment, polarizability, etc.) and in a number of cases, e.g. for molecules with a relatively large length-to-width ratio, a stabilization of the solvent ordering and an increase of T_{NI} can occur.[5] Although the molecular mechanism for the solute-solvent interaction is far from clear, a relation to molecular shape is often invoked;[6] in this context, a particularly interesting case is that of azobenzene derivative (AB) solutes, where it is possible to drive a change in shape by photoexciting the *trans* to *cis* transformation, by exposing the solution of AB to a near UV light.

The process of photoisomerization in the gas phase and to a minor extent in solution has been the object of a huge amount of basic studies (see e.g.[7–11] and refs. therein). The transformation of AB in nematics and even more in LC elastomers has in recent years received considerable interest also from the applicative point of view.[12–14] In LC elastomers containing AB units the photoisomerization can produce changes in elongation of samples up to 20%, opening the way to the realization of photodriven actuators, valves and other devices. Both from the point of view of these applications and from a more basic standpoint, it is crucial to understand how the AB isomerization acts on the surrounding medium affecting its ordering properties. While the change of T_{NI} of an AB solution in nematics following photoexcitation has been demonstrated,[15,16] a study of the way the order and the local dynamics ("rotational microviscosity") are influenced is, to our knowledge, still lacking. In this study we have then decided to investigate these changes by considering a series of AB compounds of similar shape but with varying chemical properties. In particular, we have studied seven *p*-substituted AB, shown in Figure 1a, in the nematic 4-cyano-4′-n-pentylbiphenyl (5CB, Figure 1b). We have then considered solutions of *trans* isomers of these compounds at two different concentrations (1% and 7% mole fraction) and we have followed the changes with temperature of the order and the dynamics of the medium, as experienced by a nitroxide spin probe, using the well established ESR spin probe methodology,[17–20]

also used to study azobenzene LC polymers.[21] We have then generated in situ *cis* isomer solutions, as described in the Experimental Section, and we have repeated the temperature dependent measurements. In the Results section, we present our results and compare them, showing that the effect of solutes does not always reduce to a simple scaling of the order plot, as expected when only T_{NI} is affected. On the contrary, in some cases the effect on the order is more profound with a change of the functional dependence of $\langle P_2 \rangle$ on the temperature. Finally, in the Discussion section, we try to relate the results to molecular features of the solutes studied.

Experimental Section

Materials and Methods

The structure of the photoactive units used in this study was 4-R-phenylazobenzene (see Figure 1a), where R = H, F, Br, CH_3, CF_3, O*n*-Bu, O*t*-Bu. None of the azo-derivatives considered showed a LC phase. Azobenzene was purchased from Aldrich and used without further purification. The azo-derivatives were synthesized according to the Mills reaction,[22] in which nitrosobenzene combines with primary arylamines in glacial acetic acid to give unsymmetrical azo-derivatives. The synthesis and characterization of 1-[4-(*tert*-butoxy)phenyl]-2-phenyldiazene (4-O*t*-Bu-phenylazobenzene) is original and is reported in the subsection below. The liquid crystal 5CB was used as host matrix (Figure 1b). This compound exhibits, on heating, the following phase sequence: Crystal–N (295.7 K), N–I (308.5 K). It was purchased from Merck KGaA (Darmstadt, Germany) and was used without any further purification. The nitroxide free radical used in this study was the 3β-DOXYL-5α-cholestane (CSL), purchased from Aldrich. It was chosen because it has been proven[19,23] to be a reliable probe to monitor the order and the dynamics of the LC system, due to its size, rigidity and rod-like shape analogous to that of the 5CB. The CSL structure is shown in Figure 1c together with the chosen ordering (x, y, z, solid line) and magnetic (x', y', z', dashed line) molecular frames and the indication of its two main reorientational motions, tumbling and spinning, with their respective rotational diffusion tensor principal components $D_\perp$ (reorientation of the molecular long axis) and $D_\parallel$ (rotation around the long axis).

The magnetic frame (x', y', z') was chosen according to the standard system of coordinates

for the N-O paramagnetic moiety with the x' axis along the N-O bond[19,24] and the z' axis perpendicular to the five-membered ring, i.e. parallel to the pz orbital containing the unpaired electron density. According to a standard approach, the z axis of the ordering frame is considered parallel to the principal axis of inertia of the probe and, to simplify the rotation which takes the ordering into the magnetic frame,[19] the y axis is considered parallel to the z' axis. The tilt angle β between the molecular frames, in agreement with previous works,[19,23,24] was consistently found to be $13 \pm 2°$ in the nematic (N) phase and $15 \pm 2°$ in the isotropic (I) phase, in a series of preliminary fits, and was then fixed to these values.

Samples were prepared by adding in turn one of the seven azo derivatives, at 1% and 7% mole fraction, to a solution of CSL spin probe in 5CB at a concentration of 6×10^{-4} g_{CSL}/g_{5CB}. Given the good solubility of the spin probe and of the azo-derivatives in 5CB at the concentrations studied, mechanical mixing at a temperature slightly above T_{NI} was sufficient to prepare uniform samples without adding any solvent. Fresh samples not requiring photoisomerization (*trans* isomers) were inserted into glass capillaries of 1.8 mm internal diameter and stored in the dark at room temperature until ESR measurements. To obtain the *cis* isomers, samples were treated as described later in this section. Immediately after the isomerization, they were inserted into the capillaries and ESR spectra were recorded.

We acquired ESR spectra with a Bruker ESP300E spectrometer equipped with an ER 041XG microwave X-band (9.5 GHz) Gunn Diode bridge and a rectangular ER 4102 cavity. The samples were thermostated with a nitrogen flux through a variable temperature unit Bruker B-VT 2000. The temperature, monitored with a calibrated type T thermocouple (Comark Ltd.) kept in contact with the capillary containing the sample, showed a stability better than $\pm$ 0.05 K. We recorded ESR spectra on heating taking the samples from the N to the I phase, in a range of about 20 K around T_{NI}.

The *trans–cis* photoisomerization reactions (see Figure 1a) were carried out by exposing the samples in a quartz cuvette to UV-light (λ=365 nm) with a UVGL-58 MINERALIGHT Lamp (UVP). During the exposure, we recorded several UV-visible absorption spectra with a Cary 1E (Varian) spectrophotometer to follow the *trans–cis* photoisomerization. UV-visible spectra were taken before any irradiation and after different times of exposure, diluting each sample in cyclohexane to achieve a concentration of the azo-derivative of 2.5×10^{-4} M. The *trans* isomer spectra exhibited features characteristic of *trans*-azobenzene type molecules, i.e.

a strong absorption band at about 340 nm, due to $\pi \rightarrow \pi^*$ transition, and a much weaker band centered at 450 nm, due to $n \rightarrow \pi^*$ transition. Irradiation at 365 nm caused a decrease of the $\pi \rightarrow \pi^*$ band intensity and a build-up of the $n \rightarrow \pi^*$ band, which was slightly shifted toward shorter wavelengths. This indicated that the isomerization was taking place. We considered the process successful when we could not observe any further change by comparing two consecutive UV-visible spectra (see Figure 2). This typically required between 10 and 24 hours, depending on the azo-derivative concentration. After the ESR measurements of the samples doped with the *cis* azo-derivatives, a further UV-visible absorption spectrum was taken and compared to the one taken immediately before the ESR measurements. In all the cases, these spectra were essentially identical, indicating that the *cis* isomers did not significantly reverse to the *trans* configuration during the ESR spectra acquisition.

The presence of non-mesomorphic solutes in a nematic LC can lead, in a temperature range close to the T_{NI}, to the appearance of a biphasic region, consisting of both N and I phases which coexist in equilibrium.[25–27] This actually seemed to be the case for some of the samples doped with the *cis* azo-derivatives, whose ESR spectra exhibited a line shape that could be attributed to the superposition of two different spectra, one characteristic of a nematic phase and the other of an isotropic environment. To verify for all the samples the existence and the limits of the biphasic region, if any, we also performed a series of polarizing microscope observations under crossed polarizers. Every LC mixture was held in a flat quartz cell with 25 μm spacing. The inner surface of the cell was coated with polyvinyl formal and then rubbed to achieve homogeneous alignment of the LC molecules parallel to the rubbing direction. The sample was then irradiated with UV-light (λ=365 nm) to cause the isomerization, when needed, and examined with a ORTHOPLAN Leitz polarizing microscope equipped with a thermostating stage, placing the cell with the LC director at 45 degrees with respect to the polarizers. For each system, the temperature range explored was the same considered in the ESR measurements. These investigations confirmed that pure 5CB and samples doped with *trans* isomers completely turned, at the transition, into the I phase, while mixtures containing *cis* isomers exhibited, close to the T_{NI}, a biphasic region in which both N and I phases coexisted (see Figure 3 for an example relative to 5CB doped with *cis* 4-O*n*-Bu-phenylazobenzene at 7% mole fraction).

Synthesis of 1-[4-(*tert*-butoxy)phenyl]-2-phenyldiazene

Following the standard Mills reaction,[22] a solution of nitrosobenzene (0.02 mol) and 4-(*tert*-butoxy)aniline (0.015 mol) in acetic acid was refluxed for 1 hour at 90°C. 4-(*tert*-butoxy)aniline was synthesized as described[28] and nitrosobenzene was obtained from Aldrich. The excess of acetic acid was removed *in vacuo*, the residue was neutralized with an aqueous sodium carbonate solution (10%) and then extracted three times with diethyl ether. The solvent excess was removed *in vacuo* and the resulting red solid was purified on a silica column by elution with petroleum ether and an increasing diethyl ether content. This procedure gave rise to the desired 1-[4-(*tert*-butoxy)phenyl]-2-phenyldiazene with a yield of 80%. Melting points were determined on a Kofler hot-stage apparatus. ^{1}H- and ^{13}C-NMR spectra were recorded on a Varian Gemini 300. Mass spectra were recorded using a ESI Water ZQ-4000 instrument. 1-[4-(*tert*-butoxy)phenyl]-2-phenyldiazene: m.p. 46 – 47 °C; δ_C (75.4 MHz; $CDCl_3$) 29.3 (q), 79.9 (s), 123.0 (d), 124.1 (d), 124.2 (d), 129.4 (d), 130.9 (d), 148.8 (s), 153.1 (s), 158.9 (s); δ_H (300 MHz; $CDCl_3$) 7.89 (2H, m Ar.), 7.87 (2H, d, *J* 9.0 Hz A_2B_2), 7.49 (4H, m, Ar.), 7.12 (2H, d, *J* 9.0 Hz A_2B_2), 1.42 (9H, s); *m/z* 293 (M + K), 277 (M + Na), 255 (M + H), 221, 199.

Results

The ESR spectra of the spin probe showed the expected features for CSL moving in a fluid environment with a certain degree of order, similar to those observed in previous studies of cyanobiphenyl nematics or similar materials.[23,29] The simulation of the ESR spectra was carried out with an implementation of the "slow tumbling" theory developed by Freed and collaborators assuming rotational diffusion for the probe.[17,18,20] In the analysis, the fit parameters were then optimized using a modified Gauss-Newton-Marquardt non-linear least squares method.[30,31]

ESR spectra of samples that did not show phase coexistence at the polarizing microscope were analyzed using a model we developed previously.[23] Basically, the variable parameters considered are the order parameter $\langle P_2 \rangle$ (which was kept fixed to zero to model spectra in the I phase), the perpendicular component of the rotational diffusion tensor $D_\perp$ and the inhomogeneous line width T_2^{*-1}. The ratio of spinning and tumbling diffusion coefficients

$D_r = D_\parallel / D_\perp$, introduced to minimize the correlation among some of the parameters,[23] was found to be essentially temperature independent in a series of preliminary fits, with values very close to those obtained for the pure 5CB, i.e. 7.1 in the N and 9.9 in the I phase. It was therefore kept fixed to these values in the final fits to further reduce the correlation among the parameters.

ESR spectra of samples that showed, at the polarizing microscope, a biphasic region in a certain range of temperatures, were fitted to a weighted sum of two spectra, one for each phase, both modeled with the same set of parameters described above. The weight of each spectrum was assumed to be proportional to the fraction of the nematic (f_N) or isotropic (f_I) phase present in the sample, with $f_N + f_I = 1$. In Figure 4 we show typical experimental ESR spectra and fits of a sample doped with *cis* 4-CH_3-phenylazobenzene at 7% mole fraction at temperatures representative of the N phase, of the I phase and of the biphasic region. The very good fits obtained confirmed the validity of the model.

The fraction of each phase could be estimated by using the lever rule in a temperature-composition phase diagram.[4] We illustrate the method employed in Figure 5, where we report, as an example, the phase diagram of 5CB doped with 4-O*n*-Bu-phenylazobenzene in its *cis* form. By inspection of the ESR line shapes we have detected the biphasic region limits, marked in Figure 5 as dots on the isopleth lines at 1% and 7% mole fraction, and we have then identified the α and β lines (assumed to be straight lines at low solute concentration),[2,26] which represent the composition of the N and the I coexisting phases, respectively. Considering for example the heating process of the nematic system at 7% mole fraction, at T_α the I phase begins to appear while at T_β the N phase completely vanishes. At every temperature T_j inside the coexistence range, we drew the corresponding tie line (of total length $l_N + l_I$) and applied the lever rule: $l_I f_N = l_N f_I$. We thus calculated the values of $f_N = l_N/(l_N + l_I)$ and $f_I = l_I/(l_N + l_I)$, which represent the relative amount of N and I phase in equilibrium within the biphasic region. Moreover, the intersection between the α and β lines with the tie line allowed to find out the composition of the nematic, $x^{(N)}$, and isotropic, $x^{(I)}$, coexisting phases, respectively.

To establish a uniform notation for the different samples, hereafter we shall refer to T_{NI} as to the highest temperature at which the N phase is still present in the sample, to ΔT_{NI} as to the difference between the T_{NI} of the system considered and that of the pure 5CB and to ΔT_{coex} as to the range of the biphasic region of the mixtures containing the *cis* isomers.

As reported in Table I, all the azo-doped samples studied showed a T_{NI} lower than that observed in the pure 5CB and a T_{NI} shift which increased with the concentration of the azo-derivative and was larger, at the same concentration, for the *cis* isomers. We found, in particular, ΔT_{NI} values for the *trans* isomers in the range -0.4 to -1.6 K at 1% mole fraction, increasing, in absolute value, at 7% to the range -0.7 to -8.0 K and, for the *cis* isomers, in the range -1.7 to -3.7 K and -7.9 to -19.5 K at 1% and 7% mole fraction, respectively. The ΔT_{coex} of the *cis*-doped samples, also shown in Table I, increased with the azo-derivative concentration from 0.2 to 0.6 K at 1% to the range 0.4 to 8.3 K at 7% and was wider in samples with larger ΔT_{NI}.

In Figure 6a we show our results for the order parameter $\langle P_2 \rangle$ of the spin probe against reduced temperature $T^* = T/T_{NI}$ in samples containing the *trans* isomers at 1% mole fraction. As we can see, the values are nearly identical to those relative to the pure 5CB and this can be also observed at the higher 7% mole fraction (Figure 6b), with only a very small decrease of the $\langle P_2 \rangle$ values in the samples containing the O*t*-Bu and F substituted azo-derivatives. For the *cis* isomers, the deviations are relatively larger. As shown in Figure 7a, even at 1% mole fraction all the samples show a degree of order lower than that of the pure 5CB and this decrease becomes even more evident at 7% mole fraction for all the azo-derivatives (see Figure 7b) and is particularly large in samples containing the O*n*-Bu and O*t*-Bu substituted azo-derivatives. The $\langle P_2 \rangle$ temperature dependence, in this latter case (Figure 7b), seems to have a peculiar trend. In the temperature range far from the corresponding T_{NI}, the order parameter of the various samples decreases with increasing temperature but, approaching the T_{NI}, the degree of order exhibits a small increase and then it decreases again, eventually showing the discontinuity characteristic of the N–I phase transition, once the T_{NI} is reached.

The reason for this behavior is related to the formation of the biphasic region and on the consequent partition of the *cis* azo-derivatives within the two phases. To clarify this point, it is useful to refer again to the phase diagram in Figure 5, considering the isopleth at 7% and a heating process raising the system temperature from T_α to T_β. Within the biphasic region ($T_\alpha < \mathrm{T} < T_\beta$), the solute is distributed between the N and the I phase in different proportions. At the generic temperature T_j, for instance, the *cis* azo-derivative mole fraction dissolved into the N phase, $x^{(N)}$, is smaller than the nominal concentration of 7%. Thus, in the coexistence region, the order of the N phase present in the system is the

result of the competition of two opposite temperature-related processes. On the one hand, in fact, increasing the temperature causes a higher disorder of the N phase and a lower order parameter but, on the other hand, it is the driving force for the diminishing of the *cis* isomer concentration in the nematic fraction, resulting in a smaller perturbation of the system and thus in an increase in the degree of order. The $\langle P_2 \rangle$ behavior shown in Figure 7b is then the result of these two contributions.

Such a peculiar trend of the order parameter is similar to that obtained by Polson and Burnell[32] in a Monte Carlo simulation study, investigating the $\langle P_2 \rangle$ behavior at the beginning of the nematic–isotropic coexistence region of a binary LC mixture with a Lebwohl Lasher model. Experimentally not much is available. However, in an NMR study of 5CB deuterated in different positions, Beckmann *et al.*[33] found that, in the presence of an unknown impurity at low concentration (traces), the nematic order parameter was almost constant in a portion of a relatively narrow coexistence region. It is not too surprising that, in that case,[33] in the two-phase region the order parameter has been found to be a universal function of T/T_{NI}. IIowever, in our case, at 7% of the *cis* isomer (Figure 7b), it is no longer possible to assume the order parameter as a universal function of T/T_{NI}, since it is quite evident that, already before the occurrence of the two-phase region, the order parameter is depressed by the presence of the azo-derivative beyond the expected value.

The recovery of meaningful and uncorrelated values of the nematic parameters from the fit was not possible when the nematic contribution to the biphasic ESR spectrum became too weak. Therefore, in Figure 7b, the $\langle P_2 \rangle$ values of samples with a fraction f_N lower than about 0.15 are not shown.

Surprisingly, in the preliminary fits, the dynamics seemed to be essentially independent of the nature, the configuration and the concentration of the different azo-derivatives. In particular, it appeared reasonable to assume for all the different nematic or isotropic regions, respectively, a common temperature dependence of the tumbling diffusion coefficient $D_\perp$. Therefore, in the final fits, also the $D_\perp$ was considered as a global parameter, assuming, for all the N or I phases, respectively, a simple Arrhenius-type temperature dependence ($D_\perp = D_0 \times \exp[-E/RT]$). The temperature range considered for the N phases was 274.2 to 308.5 K with best fit parameters $D_0 = (6 \pm 2) \times 10^7$ ns^{-1} and $E = 53 \pm 2$ kJ/mol. For the I phases, the temperature range was 280.7 to 320.5 K with best fit parameters $D_0 = (3 \pm 1) \times 10^5$ ns^{-1} and $E = 41 \pm 2$ kJ/mol. The quality of the fits with a global

$D_\perp$ was essentially the same as that obtained considering $D_\perp$ as an independent parameter, thus confirming the validity of our assumption.

Discussion

It is interesting to try and relate the changes induced by the solute on $\langle P_2 \rangle$ and T_{NI} from those observed for the pure 5CB to the solute-solvent interactions occurring between the different azo-derivatives and the LC host and here we wish at least to start tackling the problem. We begin discussing the overall effect of the various solutes on the ΔT_{NI} and the $\langle P_2 \rangle$ dependence on T^*. We then offer a detailed comparison of the differences in the ΔT_{NI}, due to the type of azo-derivative, for each isomer configuration and at the two mole fractions studied. Considerations based on solute shape and size (essentially "short-range" interactions) that are able to rationalize, at least in part, the N phase stability sequence of the various *cis* isomers are not valid for the *trans*, which exhibit quite a different sequence. To investigate the role of interactions at longer range, we then proceed to compare the electrostatic properties of the solutes with those of the solvent, beginning with the molecular dipole and quadrupole and then performing a qualitative comparison of the electrostatic potential at the molecular surface.

By recalling the results presented in the previous section, a first, general observation is that the *cis* isomers (V-shaped) always produce a shift of the nematic–isotropic transition to a lower temperature larger than that of the *trans* (rod-like).

At 1% and 7% *trans* and at 1% *cis*, the destabilization causes only a T_{NI} shift while the $\langle P_2 \rangle$ dependence on T^* is either completely unaffected (*trans* isomers at both mole fractions, Figure 6), or shows only a small decrease (*cis* isomers at 1%, Figure 7a). At 7% *cis*, instead, the shift to a lower temperature is no longer able to "compensate" the destabilization introduced by the azo-derivatives so that also the order of the phase is significantly depressed, compared to that of the pure 5CB, with relatively large differences among the $\langle P_2 \rangle$ vs. T^* plots (Figure 7b). By listing the derivatives, starting from the one which causes the largest decrease of $\langle P_2 \rangle$, we have the following sequence: O*t*-Bu, O*n*-Bu, CH_3, F, H, Br and CF_3. Interestingly, if we consider the T_{NI} shifts, again starting from the largest one, we have almost the same sequence, apart from the inversion of CF_3 with Br. At 1% *cis*, we also observe a similar result: O*t*-Bu, O*n*-Bu, CH_3, H, F, Br and CF_3. The sequence of stability

of the *trans* isomers is, instead, quite different from that of the *cis*. At 7% it is: H, O*t*-Bu, CF_3, F, Br, CII_3 and O*n*-Bu and it remains similar at 1%: II, O*t*-Bu, F, CF_3, Br, CII_3 and O*n*-Bu.

We can now summarize the above observations. The *cis* isomers determine an overall larger destabilization and, within the *cis* series, it seems that the destabilizing effect due to the bulkiness of the substituent is dominant (O*t*-Bu and O*n*-Bu) and, at 7% mole fraction, it affects not only the shift of the T_{NI} but also the order of the phase in a very similar way. This is compatible with the idea that the main influence on the N phase stability is played by the solute molecular shape and is also in agreement with experimental studies and simulations dealing with the orientational ordering of solutes in nematic LC and hinting that the short-range interactions, which depend on the size and on the molecular shape, strongly influence the orientational behavior of molecules in nematic solvents.[6,34] Clearly, these considerations of size are not sufficient by themselves to account for the sequence of stability observed, otherwise the unsubstituted azobenzene and the 4-F-phenylazobenzene, in the sequence of the *cis* at 7%, would have occupied the last position and the CII_3 azo-derivative, having approximately the same size as the Br or the CF_3, would have shown a similar behavior. Moreover, in the case of the *trans* isomers, it seems that the destabilizing contribution due to the larger substituents is less important since, e.g., the unsubstituted azobenzene and the O*t*-Bu azo-derivative affect the T_{NI} in a similar way. We also observe that, since the solute has a size and shape approximately corresponding to that of the solvent, the N phase is almost unaffected by its presence: indeed at both the concentrations studied, the *trans* O*n*-Bu-phenylazobenzene induces only a small T_{NI} shift.

Another relevant contribution to the orientational ordering involves long-range, solute-solvent electrostatic interactions.[6,34–36] To investigate their role, we have calculated and compared the dipole moment and the principal components of the quadrupole tensor of both the solvent and the solute molecules. For all the compounds studied, we performed a preliminary quantum mechanical DFT B3LYP/6-31G** geometry optimization and vibrational frequency calculation. Then, by using this optimized geometry, we determined, using the more extended "augmented correlation-consistent polarized valence orbital basis set of triple zeta quality" (AUG-cc-PVTZ), the dipole and quadrupole moments and the atomic point charges with the Merz-Singh-Kollman scheme, considering the additional constraint of reproducing the total molecular dipole moment.[37] The results of these calculations are

reported in Table II and Table III. Unfortunately, it was not possible to find a simple correlation between the degree of destabilization caused by the various azo-derivatives and their dipole moments or quadrupole tensor principal values, also when comparing them to those of the 5CB liquid crystal. In a way this is not surprising, since for molecules in close contact like those in a condensed phase, the full charge distribution should be considered[38] and it is not sufficient to simplify the electrostatic host-guest interactions using low rank multipole terms.

The importance of the role played by long-range interactions on the molecular orientation mechanism in nematics has been discussed in several works, particularly by Burnell *et al.* (see e.g.[35] and refs. therein), and it has been related to the average electric field arising from the charge distribution of the solvent molecules surrounding the solute and to the corresponding field gradient, experienced by the solute. Here, for each molecular species studied, we have calculated the electrostatic potential at the molecular surface (EP map) defined by the overlap of the Van der Waals spheres centered on each atom, using the simple Coulombic relation:

$$V(\mathbf{r}) = \sum_i q_i \frac{1}{|\mathbf{r} - \mathbf{r}_i|} \tag{1}$$

where $\mathbf{r}$ is the position on the molecular surface and q_i is the point charge located on the i-th atom at $\mathbf{r}_i$.

We now wish to perform a qualitative comparison between the EP map of 5CB and the map of each azo-derivative looking for features which could hint at a favorable or disruptive short-range arrangement of the solute-solvent pair and thus indirectly be related to a higher or a lower degree of destabilization for that derivative. In Figure 8, we compare the potential map of 5CB with the *trans* isomers and we consider the two extreme azo-derivatives in the sequence of stability. We see that the EP map of 5CB (Figure 8a) exhibits a strong negative site located on the CN group and a positively charged region on the alkyl chain. The EP map of the 4-O*n*-Bu-phenylazobenzene (lowest destabilization, Figure 8b) also exhibits quite a well defined positive region on the *n*-Bu group and a negative region centered on the azoic group. The similarity of shapes and EP maps hints that the introduction of this solute should be relatively innocuous on the local environment. The EP map of the unsubstituted azobenzene (highest destabilization, Figure 8c) appears instead to be quite different from

that of 5CB, being symmetrical and without distinct regions of opposite charge, suggesting a local perturbation of the solvent-solvent interactions. By considering these two compounds as the "limiting" cases for the *trans* azo-derivatives and by ordering all the other derivatives according to the intermediate features of their map, it is actually possible to recover the same sequence of stability observed experimentally, thus confirming our assumption that azo-derivatives with an EP map more similar to that of 5CB will introduce a lower degree of destabilization.

This qualitative argument is tenable only for molecules of similar shape, where the electrostatic contribution can operate a second level selection. Thus a direct comparison of the EP map of 5CB with the maps of the *cis* azo-derivatives (Figure 8d and 8e) would be more difficult due to their bent shape. However, it is still possible to observe analogous features among the *cis* azo-derivatives EP maps which can be consistently related to the different degrees of destabilization introduced in the N phase. The EP maps of the *cis* azo-derivatives responsible of the lowest and the highest degree of destabilization at 7% mole fraction are shown in Figure 8d and 8e. In the first case (Br azo-derivative), the substituent exhibits EP values close to zero, while the atoms closest to the azoic group have strongly positive values. In the second (O*t*-Bu azo-derivative), we observe a strong negative site on the *tert*-butoxy group and a relatively neutral region on the aromatic carbons bound to the azoic group. Also in this case, we ordered the other *cis* azo-derivatives according to their map and we obtained the same sequence of stability observed experimentally.

Conclusions

We have studied a series of seven closely related azobenzene derivatives, in their *trans* and *cis* form, dissolved at a mole fraction of 1% and 7% in the nematic 5CB liquid crystal. One of the aims of our study was to investigate if *trans* and *cis* azo-derivatives simply act on a nematic solvent by shifting T_{NI}[15,16] or if more subtle effects come into play. We have found that the presence of the azo-derivative caused, in all the present cases, a depression of the T_{NI}. The *cis* isomers reduced the order of the 5CB nematic phase and induced a larger T_{NI} shift with respect to the *trans* isomers. At higher mole fraction, we observed an analogous behavior with larger effects. At both concentrations of the *trans* isomers and at 1% of the *cis*, the T^* dependence of our spin probe order parameter remained unchanged by the addition

of the solute with respect to that of the pure 5CB. At 7% *cis* isomers, instead, the $\langle P_2 \rangle$ decreased significantly, indicating a more unexpected and profound change of the functional dependence of $\langle P_2 \rangle$ on the temperature and on the chemical nature of the azo-derivative. In the presence of the *cis* isomers the samples showed a region of phase separation which was almost negligible at 1% but became quite evident at 7% and was found to be wider in samples with larger T_{NI} shifts.

The $\langle P_2 \rangle$ recovered after suitable allowance for the biphasic region in simulating the probe spectra showed a peculiar dependence on T^* with the order parameter slightly increasing as the system enters the biphasic region. It is important to notice that, even setting aside the region very close to T_{NI}, the order parameter of the *cis* isomers showed marked changes for the different substituents, with a more pronounced effect for the alkoxy groups.

Surprisingly, the rotational dynamics of the probe, and thus indirectly the local rotational microviscosity, appeared to be unaffected by the nature, the isomer type or the concentration of the different azo-derivatives.

We discussed also the possibility of relating the different degrees of destabilization to long-range electrostatic interactions of 5CB with the different azo-derivatives. No simple correlation was found with the low rank electrostatic terms (molecular dipole or quadrupole). However, interesting structure-stability correlations were found considering the full electrostatic potential maps of 5CB and of the different solutes, indicating that, at least for comparable shapes and sizes, an azo-derivative with a potential map more similar to that of the 5CB will introduce a lower degree of destabilization in the phase.

We believe that further, more quantitative advances will be obtainable only with realistic Molecular Dynamics simulations of the guest-host interactions, together with predictions of the nematic–isotropic transition temperature that are now starting to become feasible.[39] A similar approach goes well beyond the scope of this article and it would represent a complete new study in itself which we plan to carry on in a following work.

Even without this full understanding of the effects of the solute structure on the nematic solvent, we believe that our findings, i.e. that (*i*) the changes in order induced by the *cis* isomers go beyond a simple shift in transition and that (*ii*) it is possible to obtain substituent dependent differences of up to 25% in the ordering, should be of interest in photonic applications based on the azobenzene photoresponsive properties.

Acknowledgments

We thank MIUR (PRIN "Modelling and characterisation of liquid crystals for nano-organised structures" and FIRB "Molecular and organic/inorganic hybrid nanostructures for photonics"), INSTM and the University of Bologna for support. We also thank Prof. F. Bertinelli and Prof. M. G. Giorgini for the use of the polarizing microscope and the relative thermostating unit.

[1] Schadt, M.; Mueller, F. *J. Chem. Phys.* **1976**, *65*, 2224.

[2] DasGupta, S.; Chattopadhyay, P.; Roy, S. K. *Phys. Rev. E* **2001**, *63*, 041703/1.

[3] Syvitski, R. T.; Pau, M.; Burnell, E. E. *J. Chem. Phys.* **2002**, *117*, 376.

[4] Martire, D. E. In *The Molecular Physics of Liquid Crystals*; Luckhurst, G. R., Gray, G. W., Eds.; Academic Press: London, 1979.

[5] Sigaud, G.; Achard, M. F.; Hardouin, H.; Gasparoux, H. *Chem. Phys. Lett.* **1977**, *48*, 122.

[6] Burnell, E. E.; de Lange, C. A. *Chem. Rev.* **1998**, *98*, 2359.

[7] Cattanco, P.; Persico, M. *Phys. Chem. Chem. Phys.* **1999**, *1*, 4739.

[8] Ciminelli, C.; Granucci, G.; Persico, M. *Chem. Eur. J.* **2004**, *10*, 2327.

[9] Cembran, A.; Bernardi, F.; Garavelli, M.; Gagliardi, L.; Orlandi, G. *J. Am. Chem. Soc.* **2004**, *126*, 3234.

[10] Chang, C.-W.; Lu, Y.-C.; Wang, T.-T.; Diau, E. W.-G. *J. Am. Chem. Soc.* **2004**, *126*, 10109.

[11] Crecca, C. R.; Roitberg, A. E. *J. Phys. Chem. A* **2006**, *110*, 8188.

[12] Ichimura, K. *Chem. Rev.* **2000**, *100*, 1847.

[13] Finkelmann, H.; Nishikawa, E.; Pereira, G.; Warner, M. *Phys. Rev. Lett.* **2001**, *87*, 015501(4).

[14] Hubert, C.; Rumyantseva, A.; Lerondel, G.; Grand, J.; Kostcheev, S.; Billot, L.; Vial, A.; Bachelot, R.; Royer, P.; Chang, S. H.; Gray, S. K.; Wiederrecht, G. P.; Schatz, G. C. *Nanoletters* **2005**, *5*, 615.

[15] Ikeda, T. *J. Mater. Chem.* **2003**, *13*, 2037.

[16] Tsutsumi, O.; Shiono, T.; Ikeda, T.; Galli, G. *J. Phys. Chem. B* **1997**, *101*, 1332.

[17] Freed, J. H. In *Electron Spin Relaxation in Liquids*; Muus, L. T., Atkins, P. W., Eds.; Plenum Press: New York, 1972; chapter 14, page 387.

[18] Freed, J. H. In *Spin Labeling. Theory and Applications*; Berliner, L. J., Ed.; Academic Press: New York, 1976; chapter 3, page 53.

[19] Meirovitch, E.; Freed, J. H. *J. Phys. Chem.* **1984**, *88*, 4995.

[20] Schneider, D. J.; Freed, J. H. In *Biological Magnetic Resonance. Spin Labeling*; Berliner, L. J., Reuben, J., Eds., Vol. 8; Plenum Press: New York, 1989; chapter 1.

[21] Andreozzi, L.; Autiero, C.; Faetti, M.; Zulli, F.; Giordano, M.; Galli, G. *Mol. Cryst. Liq. Cryst.* **2006**, *450*, 163.

[22] Boyer, J. In *The Chemistry of the Nitro and Nitroso Groups*; Feuer, H., Ed., number Part 1; Interscience: New York, 1969; page 216.

[23] Arcioni, A.; Bacchiocchi, C.; Vecchi, I.; Venditti, G.; Zannoni, C. *Chem. Phys. Lett.* **2004**, *396*, 433.

[24] Carr, S. G.; Khoo, S. K.; Luckhurst, G. R.; Zannoni, C. *Mol. Cryst. Liq. Cryst.* **1976**, *35*, 7.

[25] Humphries, R.; Luckhurst, G. *Proc. R. Soc. Lond. A.* **1976**, *352*, 41.

[26] Martire, D.; Oweimreen, G.; Agren, G.; Ryan, S.; Peterson, H. *J. Chem. Phys.* **1976**, *64*, 1456.

[27] Oweimreen, G. *J. Phys. Chem. B* **2001**, *105*, 8410.

[28] Ramlall, P.; McClelland, R. *J. Chem. Soc. Perkin Trans. 2* **1999**, page 225.

[29] Arcioni, A.; Bacchiocchi, C.; Grossi, L.; Nicolini, A.; Zannoni, C. *J. Phys. Chem. B* **2002**, *106*, 9245.

[30] Arcioni, A.; Tarroni, R.; Zannoni, C. *J. Chem. Soc. Faraday Trans.* **1993**, *89*, 2815.

[31] Bevington, P. R. *Data Reduction and Error Analysis for the Physical Sciences;* McGraw-Hill: New York, 1969.

[32] Polson, J. M.; Burnell, E. E. *Chem. Phys. Lett.* **1997**, *281*, 207.

[33] Beckmann, P. A.; Emsley, J. W.; Luckhurst, G. R.; Turner, D. L. *Mol. Phys.* **1986**, *59*, 97.

[34] Syvitski, R. T.; Burnell, E. E. *J. Chem. Phys.* **2000**, *113*, 3452.

[35] Syvitski, R. T.; Burnell, E. E. *Chem. Phys. Lett.* **1997**, *281*, 199.

[36] Dingemans, T.; Photinos, D. J.; Samulski, E. T.; Terzis, A. F.; Wutz, C. *J. Chem. Phys.* **2003**, *118*, 7046.

[37] Cornell, W. D.; Cieplak, P.; Bayly, C. I.; Gould, I. R.; Merz, J. K. M.; Ferguson, D. M.; Spellmeyer, D. C.; Fox, T.; Caldwell, J. W.; Kollman, P. A. *J. Am. Chem. Soc.* **1995**, *117*, 5179.

[38] Berardi, R.; Muccioli, L.; Orlandi, S.; Ricci, M.; Zannoni, C. *Chem. Phys. Lett.* **2004**, *389*, 373.

[39] Berardi, R.; Muccioli, L.; Zannoni, C. *Chem. Phys. Chem.* **2004**, *5*, 104.

TABLES

TABLE I: Effect of the *trans* and *cis* *p*-azobenzene derivatives at 1% and 7% mole fraction on the nematic phase stability[a]

R[b]	T_{NI}/K				ΔT_{NI}/K				ΔT_{coex}/K	
	trans		*cis*		*trans*		*cis*		*cis*	
	1%	7%	1%	7%	1%	7%	1%	7%	1%	7%
O*t*-Bu	307.3	301.3	304.8	289.0	−1.2	−7.2	−3.7	−19.5	0.6	8.3
O*n*-Bu	308.1	307.8	304.9	291.9	−0.4	−0.7	−3.6	−16.6	0.6	5.2
CH_3	308.1	306.4	305.6	294.5	−0.4	−2.1	−2.9	−14.0	0.5	1.9
F	307.4	302.7	305.8	295.6	−1.1	−5.8	−2.7	−12.9	0.3	0.8
H	306.9	300.5	305.7	295.7	−1.6	−8.0	−2.8	−12.8	0.2	0.7
CF_3	307.5	302.0	306.8	299.5	−1.0	−6.5	−1.7	−9.0	0.2	0.4
Br	308.0	305.2	305.9	300.6	−0.5	−3.3	−2.6	−7.9	0.2	0.5
5CB	308.5									

[a]Abbreviations: T_{NI}, nematic–isotropic transition temperature; $\Delta T_{NI} = T_{NI,5CB+azo} - T_{NI,5CB}$, shift of the T_{NI} relative to the pure 5CB; ΔT_{coex}, nematic–isotropic coexistence range.

[b]Substituent of the azo-derivative.

TABLE II: Dipole moment (μ) and dipole components (μ_i) of the various molecular species used in this study[a]

R[b]	*trans*				*cis*			
	μ	μ_x	μ_y	μ_z	μ	μ_x	μ_y	μ_z
O*t*-Bu	1.66	-0.96	-0.11	1.35	3.26	-2.24	-2.37	0.15
O*n*-Bu	2.50	2.27	-1.05	0.00	4.39	3.61	2.44	0.55
CH_3	0.81	-0.81	-0.06	0.00	3.63	-1.10	-3.45	0.21
F	1.52	-1.51	0.21	0.00	2.34	0.69	-2.23	0.23
H	0.00	0.00	0.00	0.00	3.17	0.00	-3.17	0.00
CF_3	3.64	3.63	0.19	-0.08	2.66	-1.96	-1.78	-0.24
Br	1.89	-1.89	0.14	0.00	2.39	0.54	-2.31	0.31
5CB	6.32	6.26	0.61	0.64				

[a]Values calculated at B3LYP/6-31G** – AUG-cc-PVTZ level in the molecular inertial frame and expressed in Debye.

[b]Substituent of the azo-derivative.

TABLE III: Quadrupole components Q_{ii} of the various molecules used in this study[a]

R[b]	*trans*			*cis*		
	Q_{xx}	Q_{yy}	Q_{zz}	Q_{xx}	Q_{yy}	Q_{zz}
O*t*-Bu	13.7	0.2	-13.9	13.4	-15.8	2.4
O*n*-Bu	15.1	-2.4	-12.7	16.8	-16.2	-0.6
CH_3	12.9	-0.3	-12.6	9.8	-8.8	-1.0
F	1.1	6.6	-7.6	11.5	-12.7	1.2
H	10.9	1.1	-12.0	9.3	-7.8	-1.5
CF_3	0.0	7.3	-7.3	-17.0	13.4	3.6
Br	5.9	3.7	-9.6	12.2	-14.0	1.8
5CB	-35.8	24.1	11.7			

[a]Values calculated at B3LYP/6-31G** – AUG-cc-PVTZ level in the quadrupolar frame and expressed in Debye Å.

[b]Substituent of the azo-derivative.

FIGURE CAPTIONS

Figure 1. Chemical structure of (a) the photoactive units 4-R-phenylazobenzene (R = H, F, Br, CH_3, CF_3, O*n*-Bu, O*t*-Bu) together with the *trans–cis* photoisomerization scheme, (b) the 5CB liquid crystal and (c) the CSL spin probe together with the chosen ordering and magnetic molecular frames (see text for details).

Figure 2. Typical absorption spectra recorded after different times of UV exposure. Example relative to 5CB doped with 4-O*t*-Bu-phenylazobenzene dissolved in cyclohexane (see text for details).

Figure 3. Pictures of 5CB doped with *cis* 4-O*n*-Bu-phenylazobenzene at 7% mole fraction, taken with the cell between crossed polarizers (see text for details). Bright and dark areas correspond to the nematic and the isotropic phases, respectively. We show the sample at the highest temperature at which it is still completely nematic (a: $T = 286.7$ K), in the biphasic region (b: $T = 289.8$ K; c: $T = 290.8$ K) and at a temperature at which it is completely isotropic (d: $T = 292.2$ K).

Figure 4. Experimental ESR spectra (dashed line) and fits (solid line) of 5CB doped with *cis* 4-CH_3-phenylazobenzene at 7% mole fraction. For each spectrum, the temperature and the corresponding phases are indicated. For the spectra recorded in the biphasic region the fraction of the nematic phase f_N is also reported.

Figure 5. Temperature-composition phase diagram of 5CB, doped with *cis* 4-O*n*-Bu-phenylazobenzene, showing the nematic–isotropic coexistence region. Also shown are the experimental ESR spectra, at 7% mole fraction, acquired at the limiting temperatures (T_α and T_β) and approximately in the middle (T_j) of the biphasic region.

Figure 6. Order parameter $\langle P_2 \rangle$ of the spin probe against reduced temperature T^* for the samples doped with the *trans* azo-derivatives at (a) 1% and (b) 7% mole fraction, compared to the pure 5CB. The sequence of the substituents, from bottom to top in the key, is in order of increasing T_{NI}, as listed also in the arrow-shaped scheme.

Figure 7. Order parameter $\langle P_2 \rangle$ of the spin probe against reduced temperature T^* for the samples doped with the *cis* azo-derivatives at (a) 1% and (b) 7% mole fraction, compared to the pure 5CB. The sequence of the substituents, from bottom to top in the key, is in order of increasing T_{NI}, as listed also in the arrow-shaped scheme.

Figure 8. Electrostatic potential at the molecular surface for the 5CB (a), *trans* 4-O*n*-Bu-phenylazobenzene (b), *trans*-azobenzene (c), *cis* 4-Br-phenylazobenzene (d) and *cis* 4-O*t*-Bu-phenylazobenzene (e). Color coded according to the palette (units $4\pi\epsilon_0 e/\text{Å}$). Geometry and charges obtained at B3LYP/6-31G** – AUG-cc-PVTZ level.

FIGURES

(a)

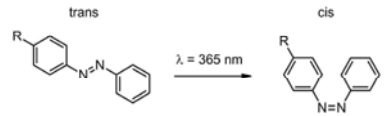

(b)

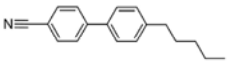

(c)

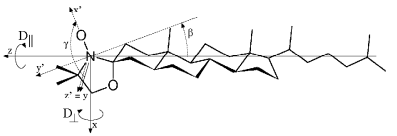

FIG. 1:

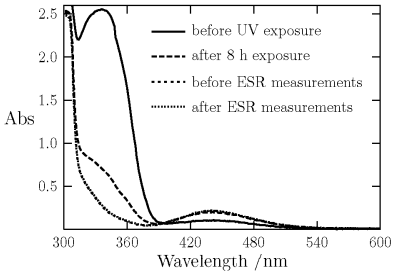
2.5
2.0
1.5
1.0
0.5
Abs
300
360
420
480
540
600
Wavelength /nm
before UV exposure
after 8 h exposure
before ESR measurements
after ESR measurements

FIG. 2:

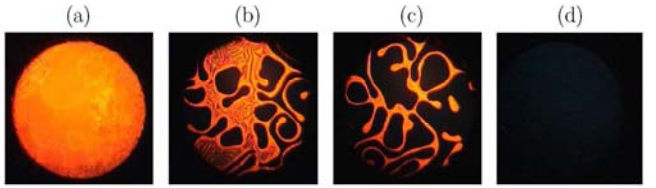
(a)
(b)
(c)
(d)

FIG. 3:

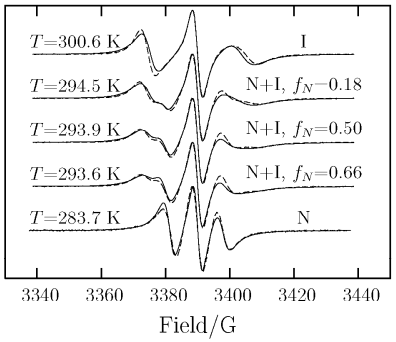
T=300.6 K
I
T=294.5 K
N+I, f_N=0.18
T=293.9 K
N+I, f_N=0.50
T=293.6 K
N+I, f_N=0.66
T=283.7 K
N
3340
3360
3380
3400
3420
3440
Field/G

FIG. 4:

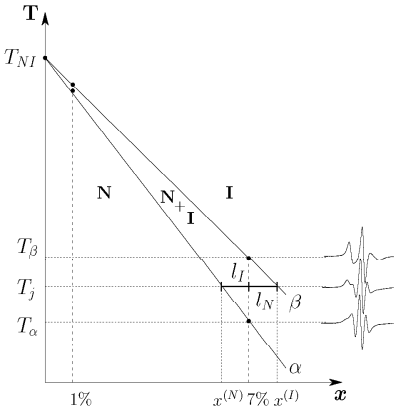
T
T_{NI}
N
N_+
I
I
T_β
T_j
T_α
l_I
l_N
β
α
1%
$x^{(N)}$
7%
$x^{(I)}$
x

FIG. 5:

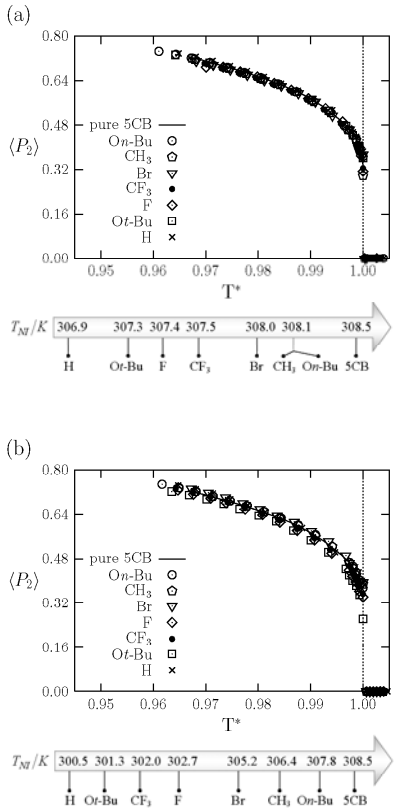
(a)
0.80
0.64
0.48
0.32
0.16
0.00
⟨P2⟩
pure 5CB
On-Bu
CH3
Br
CF3
F
Ot-Bu
H
0.95 0.96 0.97 0.98 0.99 1.00
T*
TNI/K
306.9 307.3 307.4 307.5 308.0 308.1 308.5
H Ot-Bu F CF3 Br CH3 On-Bu 5CB
(b)
0.80
0.64
0.48
0.32
0.16
0.00
⟨P2⟩
pure 5CB
On-Bu
CH3
Br
F
CF3
Ot-Bu
H
0.95 0.96 0.97 0.98 0.99 1.00
T*
TNI/K
300.5 301.3 302.0 302.7 305.2 306.4 307.8 308.5
H Ot-Bu CF3 F Br CH3 On-Bu 5CB

FIG. 6:

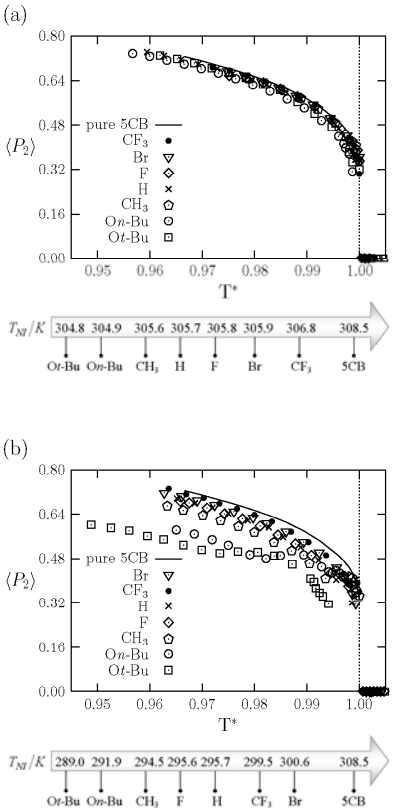
(a)
0.80
0.64
0.48
0.32
0.16
0.00
⟨P2⟩
pure 5CB
CF3
Br
F
H
CH3
On-Bu
Ot-Bu
0.95 0.96 0.97 0.98 0.99 1.00
T*
TNI/K
304.8 304.9 305.6 305.7 305.8 305.9 306.8 308.5
Ot-Bu On-Bu CH3 H F Br CF3 5CB
(b)
0.80
0.64
0.48
0.32
0.16
0.00
⟨P2⟩
pure 5CB
Br
CF3
H
F
CH3
On-Bu
Ot-Bu
0.95 0.96 0.97 0.98 0.99 1.00
T*
TNI/K
289.0 291.9 294.5 295.6 295.7 299.5 300.6 308.5
Ot-Bu On-Bu CH3 F H CF3 Br 5CB

FIG. 7:

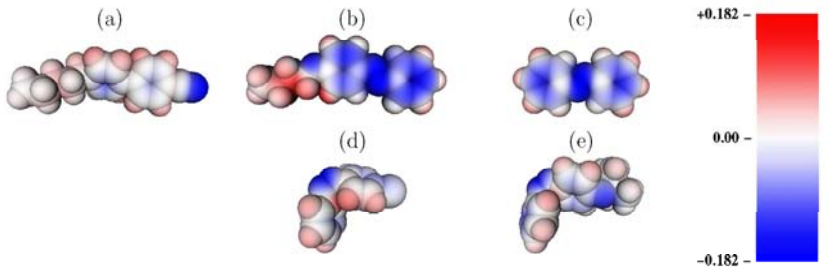

FIG. 8: